# HOKKAIDO UNIVERSITY

| Title | Multi- core fiber design and analysis : coupled-mode theory and coupled-power theory |
|---|---|
| Author(s) | Koshiba, Masanori; Saitoh, Kunimasa; Takenaga, Katsuhiro et al. |
| Citation | Optics Express, 19(26), B102-B111<br>https://doi.org/10.1364/OE.19.00B102 |
| Issue Date | 2011-12-12 |
| Doc URL | https://hdl.handle.net/2115/48130 |
| Rights | ©2011 Optical Society of America |
| Type | journal article |
| File Information | OE19-26_B102-B111.pdf |

# Multi-core fiber design and analysis: coupled-mode theory and coupled-power theory

**Masanori Koshiba,[1,*] Kunimasa Saitoh,[1] Katsuhiro Takenaga[2], and Shoichiro Matsuo[2]**

[1]*Division of Media and Network Technologies, Hokkaido University, Sapporo 060-0814, Japan*
[2]*Optics and Electronics Laboratory, Fujikura Ltd., Sakura 285-8550, Japan*
*\*koshiba@ist.hokudai.ac.jp*

**Abstract:** Coupled-mode and coupled-power theories are described for multi-core fiber design and analysis. First, in order to satisfy the law of power conservation, mode-coupling coefficients are redefined and then, closed-form power-coupling coefficients are derived based on exponential, Gaussian, and triangular autocorrelation functions. Using the coupled-mode and coupled-power theories, impacts of random phase-offsets and correlation lengths on crosstalk in multi-core fibers are investigated for the first time. The simulation results are in good agreement with the measurement results. Furthermore, from the simulation results obtained by both theories, it is confirmed that the reciprocity is satisfied in multi-core fibers.

**OCIS codes:** (060.2270) Fiber characterization; (060.2280) Fiber design and fabrication.

## References and links

1. J. M. Fini, B. Zhu, T. F. Taunay, and M. F. Yan, "Statistics of crosstalk in bent multicore fibers," Opt. Express **18**(14), 15122–15129 (2010).
2. T. Hayashi, T. Nagashima, O. Shimakawa, T. Sasaki, and E. Sasaoka, "Crosstalk variation of multi-core fibre due to fibre bend," in *Proceedings of 36th European Conference and Exhibition on Optical Communication* (Institute of Electrical and Electronics Engineers, 2010), paper We.8.F.6.
3. K. Takenaga, Y. Arakawa, S. Tanigawa, N. Guan, S. Matsuo, K. Saitoh, and M. Koshiba, "An investigation on crosstalk in multicore fibers by introducing random fluctuation along longitudinal direction," IEICE Trans. Commun. **E94-B**, 409–416 (2011).
4. S. Matsuo, K. Takenaga, Y. Arakawa, Y. Sasaki, S. Tanigawa, K. Saitoh, and M. Koshiba, "Crosstalk behavior of cores in multi-core fiber under bent condition," IEICE Electron. Express **8**(6), 385–390 (2011).
5. K. Imamura, Y. Tsuchida, K. Mukasa, R. Sugizaki, K. Saitoh, and M. Koshiba, "Investigation on multi-core fibers with large Aeff and low micro bending loss," Opt. Express **19**(11), 10595–10603 (2011).
6. K. Saitoh and M. Koshiba, "Full-vectorial imaginary-distance beam propagation method based on a finite element scheme: Application to photonic crystal fibers," IEEE J. Quantum Electron. **38**(7), 927–933 (2002).
7. A. Hardy and W. Streifer, "Coupled mode theory of parallel waveguides," J. Lightwave Technol. **3**(5), 1135–1146 (1985).
8. A. W. Snyder and A. Ankiewicz, "Optical fiber couplers-optimum solution for unequal cores," J. Lightwave Technol. **6**(3), 463–474 (1988).
9. W.-P. Huang, "Coupled-mode theory for optical waveguides: an overview," J. Opt. Soc. Am. A **11**(3), 963–983 (1994).
10. D. Marcuse, "Derivation of coupled power equations," Bell Syst. Tech. J. **51**, 229–237 (1972).
11. K. Petermann, "Microbending loss in monomode fibers," Electron. Lett. **12**(4), 107–109 (1976).
12. D. Marcuse, "Microdeformation losses of single-mode fibers," Appl. Opt. **23**(7), 1082–1091 (1984).

## 1. Introduction

Multi-core fibers (MCF) are now intensively studied for space-division multiplexing (SDM). Low-crosstalk design is indispensable for realizing SDM-based long-haul transmission. Recently, a coupled-mode theory (CMT) and a coupled-power theory (CPT) have been introduced to estimate inter-core crosstalk in various MCF [1–5]. In CMT [1,2], a phase offset between two cores is treated as a random variable because it is easily fluctuated by bending and twisting MCFs. Although average crosstalk values calculated from CMT agree well with the measurement results [2], an appropriate interval (hereafter called segment length) for applying random phase-offsets to all cores has remained unclear. Furthermore, in the earlier

CMT [1,2], conventional coupled-mode equations (CME) without higher-order terms are employed and the mode-coupling coefficients (MCC) are not symmetric. Therefore, total power may not be conserved. In CPT [3–5], on the other hand, the power-coupling coefficients (PCC) for MCF have not been fully investigated and therefore, there is about 10-dB difference between the simulation and the measurement results [4].

In this paper, first, in order to satisfy the law of power conservation, we redefine MCCs and reveal that in the CMT analysis, the crosstalk in bent and twisted MCF is strongly dependent on the segment length. Then, for the CPT analysis, we propose closed-form PCCs based on exponential autocorrelation function (EAF), Gaussian autocorrelation function (GAF), and triangular autocorrelation function (TAF) for describing random imperfections along fiber direction and reveal that the crosstalk in bent and twisted MCF is also strongly dependent on the correlation length included in the autocorrelation functions. The simulation results obtained by CMT and CPT with EAF and TAF are in good agreement with the measurement results [4]. Furthermore, from the simulation results obtained by both theories, it is confirmed that the reciprocity is satisfied in MCFs. Propagation constants of each core and MCCs between two cores in a straight MCF necessary for the solutions of CMT and CPT are accurately evaluated with the finite element method [6] which can treat measured refractive-index profiles.

## 2. Coupled-mode theory

### 2.1 Redefinition of mode-coupling coefficients

Conventional coupled-mode equations (CME) without higher-order terms for bent multi-core fibers (MCF) shown in Fig. 1(a) are written as [1,2]

$$\frac{dA_m}{dz} = -j \sum_{n \neq m} \kappa_{mn} A_n(z) \exp(j\Delta\beta_{mn}z) f(z) \tag{1}$$

where $A_m$ is the mode amplitude in core $m$, $z$ is the propagation direction, $\kappa_{mn}$ is the mode-coupling coefficient (MCC) from core $n$ to core $m$, $\Delta\beta_{mn} = \beta_m - \beta_n = -\Delta\beta_{nm}$ is the propagation-constant difference with $\beta_m$ and $\beta_n$ being the propagation constants of modes in core $m$ and core $n$, respectively, and $f$ is the phase function describing bending and twisting effects. The phase function is separated into two parts. One is the deterministic part, $\exp[j(\phi_m - \phi_n)]$, and the other is the random part, $\delta f$,

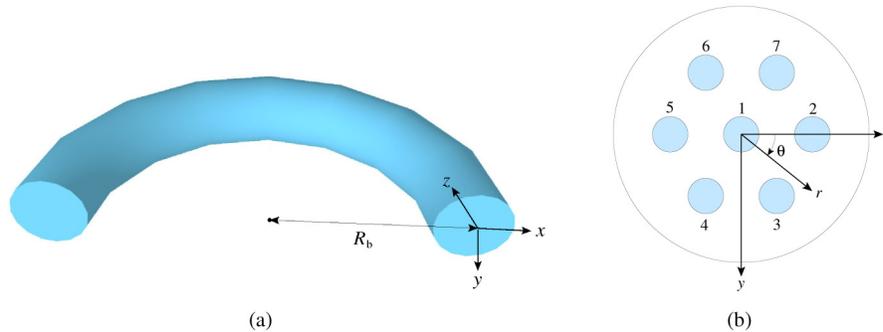$$f(z) = \exp[j(\phi_m - \phi_n)]\delta f(z) \tag{2}$$



Fig. 1. Schematics of (a) bent multi-core fiber and (b) fiber cross-section.

with $\phi_m$ being the phase in core $m$ caused by bend and/or twist. For regular 7-core fibers as shown in Fig. 1(b), $\phi_1 = 0$ and $\phi_2$ to $\phi_7$ are expressed as [2]

$$\phi_m = \int_0^z \frac{\beta_m \Lambda}{R_b(z')} \cos\theta_m(z') dz' \tag{3}$$

where $\Lambda$ is the core pitch, $R_b$ is the bending radius, and $\theta_m$,

$$\theta_m(z) = \gamma z + (m-2)\frac{\pi}{3} + \theta_0 \tag{4}$$

with $\gamma$ and $\theta_0$ being the twist pitch and the twist offset, respectively. The phase in core $m$, $\phi_m$, for arbitrarily located cores is also reported in [1].

For loss-less MCFs, MCCs should be symmetric, $\kappa_{mn} = \kappa_{nm}$. However, for non-identical cores, they are not symmetric and therefore, when using conventional CMEs, total power is not conserved. In this case, using the cross-power term, $C_{mn} = C_{nm}$, the relation between $\kappa_{mn}$ and $\kappa_{nm}$ is rewritten as [7,8]

$$\kappa_{nm} = \kappa_{mn} - C_{mn}\Delta\beta_{mn} \tag{5}$$

and the maximum power-conversion efficiency from core $n$ to core $m$ is also rewritten as [7,8]

$$F_{mn} = \frac{(\kappa_{mn} - C_{mn}\Delta\beta_{mn}/2)^2}{\kappa_{mn}\kappa_{nm} + (\Delta\beta_{mn}/2)^2} \tag{6}$$

Noting that for identical cores ($\kappa_{mn} = \kappa_{nm}$, $C_{mn} = 0$), the maximum power-conversion efficiency is reduced to

$$F_{mn} = \frac{\kappa_{mn}^2}{\kappa_{mn}^2 + (\Delta\beta_{mn}/2)^2} \tag{7}$$

We redefine MCCs as

$$K_{mn} \equiv \kappa_{mn} - C_{mn}\frac{\Delta\beta_{mn}}{2} \tag{8}$$

and

$$K_{nm} \equiv \kappa_{nm} - C_{nm}\frac{\Delta\beta_{nm}}{2} = \kappa_{nm} + C_{mn}\frac{\Delta\beta_{mn}}{2} \tag{9}$$

Considering Eq. (5), the redefined MCCs, $K_{mn}$ and $K_{nm}$, can be written as average of usual MCCs, $\kappa_{mn}$ and $\kappa_{nm}$,

$$K_{mn} = \frac{\kappa_{mn} + \kappa_{nm}}{2} = K_{nm} \tag{10}$$

The redefined MCCs are symmetric and therefore, we can use the conventional CMEs and the law of power conservation is satisfied. The average MCCs have been introduced to the analysis of propagation constants of super-modes in coupled waveguides [9] but have not been applied to power-coupling problems.

In order to consider the random part of phase function, $\delta f$, the total link is divided into finite segments of arbitrary but equal length, $d_s$, as shown in Fig. 2, and then, random phase-offsets generated by using uniform random numbers, $\exp(j\phi_{rnd})$, are applied to all cores at every segment. The segment length used in CMT is thought to be a stochastic parameter corresponding to the correlation length used in CPT.
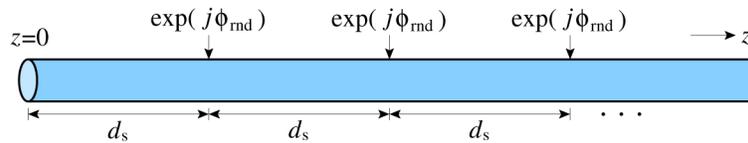
Fig. 2. Random phase-offsets applied to all cores at every segment.

## 2.2 Simulation results

We consider a quasi-homogeneous 7-core fiber as shown in Fig. 3 [4]. The core pitch is about 39.2 μm and the diameter of center core (core 1) is 8.05 μm. The diameters of outer cores are assumed to be 7.63 μm (core 2), 7.83 μm (core 3), 7.69 μm (core 4), 7.93 μm (core 5), 7.70 μm (core 6), and 7.94 μm (core 7) used for simulation in [4]. The outer cores whose diameters are categorized into two groups (cores 2, 4, and 6, and cores 3, 5, and 7) are arranged alternately circumference direction. The relative refractive-index differences of all cores are assumed to be 0.4%. The mode-field diameters range from 9.57 to 9.77 μm at a wavelength of 1550 nm.
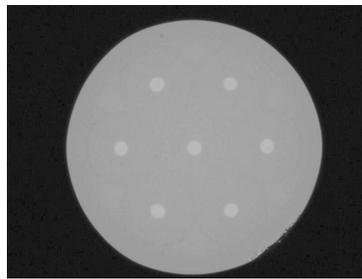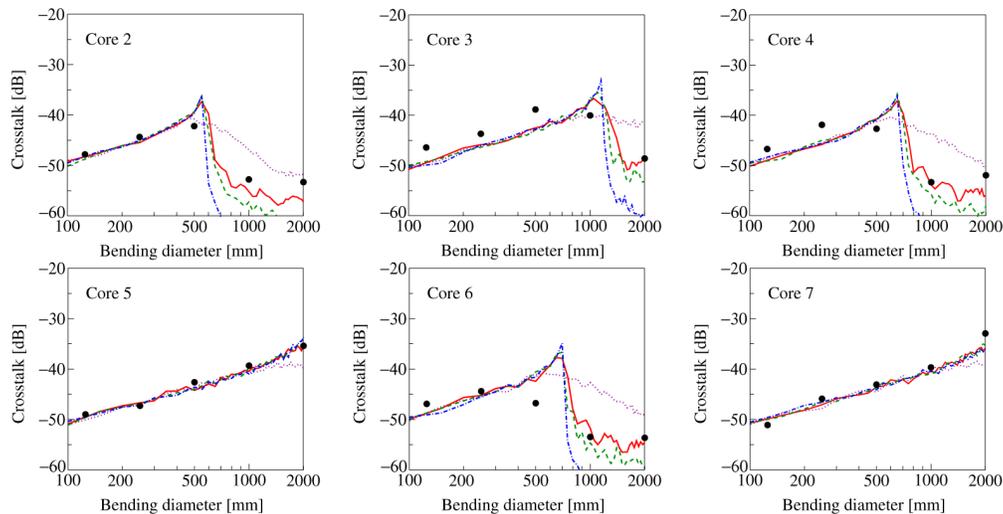


Fig. 3. Cross-section of a quasi-homogeneous 7-core fiber [4].



Fig. 4. Bending-diameter dependence of crosstalk calculated from coupled-mode theory. Dotted line: $d_s = 0.01$ m, solid line: $d_s = 0.05$ m, dashed line: $d_s = 0.1$ m, dashed and dotted line: $d_s = 0.5$ m, closed circles: measured data [4].

Figure 4 shows the bending-diameter dependence of crosstalk from center core to outer cores in the quasi-homogeneous 7-core fiber (see Fig. 3) with length of 100 m [4], where the twist rate is assumed to be 5 turns per 100 m [4] (the crosstalk distribution is less sensitive to the twist rate [2]) and the crosstalk values are averaged over 100 samples. The crosstalk is

degraded at small radii due to index-matching, in other words, phase-matching resonances between adjacent cores [1,2]. In the phase-matching region, the crosstalk is independent of the segment length and therefore, bend perturbations are crucial. In the non-phase-matching region, on the other hand, the crosstalk is strongly dependent on the segment length and therefore, the crosstalk is dominated by the statistical properties. The simulation results with $d_s = 0.05$ m agree well with the measurement results [4].

## 3. Coupled-power theory

### 3.1 Derivation of power-coupling coefficients

Coupled-power equations (CPE) are written as [10]

$$\frac{dP_m}{dz} = \sum_{n \neq m} h_{mn}(z)[P_n(z) - P_m(z)] \tag{11}$$

where $P_m$ is the average power in core $m$ and $h_{mn}$ is the power-coupling coefficient (PCC). As PCCs should be symmetric, the starting point for deriving PCCs is CMEs with redefined MCCs, $K_{mn} = K_{nm}$. In order to obtain longitudinally varying, in other words, local PCCs, considering Eq. (3) and defining the local propagation-constant difference at $z = z'$, $\Delta\beta'_{mn}$,

$$\Delta\beta'_{mn} = \Delta\beta_{mn} + \frac{\Lambda}{R_b(z')}[\beta_m \cos\theta_m(z') - \beta_n \cos\theta_n(z')] \tag{12}$$

CMEs with redefined MCCs are reduced to

$$\frac{dA_m}{dz} = -j\sum_{n \neq m} K_{mn} A_n(z) \exp(-j\Delta\beta'_{mn}z)\delta f(z) \tag{13}$$

The remaining random part of phase function, $\delta f$, is assumed to be stationary and the ensemble average is equal to zero, $\langle \delta f(z) = 0 \rangle$. Using the solutions of Eq. (13), the average power at a point $z$ sufficiently close to $z = 0$, $P_m(z) = \langle |A_m(z)|^2 \rangle$, is given by [1,10]

$$P_m(z) = \left\langle \left[ K_{mn} A_n(0) \int_0^z \exp(j\beta'_{mn}\xi)\delta f(\xi)d\xi \right] \right. $$
$$\left. \left[ K_{mn} A_n^*(0) \int_0^z \exp(-j\beta'_{mn}\eta)\delta f^*(\eta)d\eta \right] \right\rangle \tag{14}$$

Rewriting this equation as

$$P_m(z) = K_{mn}^2 P_n(0) \int_0^z d\eta \int_0^z \exp[j\Delta\beta'_{mn}(\xi-\eta)]\langle \delta f(\xi)f^*(\eta)\rangle d\xi \tag{15}$$

and changing the variable, $\zeta = \xi - \eta$, we obtain

$$P_m(z) = K_{mn}^2 P_n(0) \int_0^z d\eta \left[ \int_0^z \exp(j\Delta\beta'_{mn}\zeta)\langle \delta f(\eta+\zeta)\delta f^*(\eta)\rangle d\zeta \right] \tag{16}$$

The random part of phase function, $\delta f$, is a stationary random process and therefore, it has an autocorrelation function, $R(\zeta) = \langle \delta f(\eta+\zeta)\delta f^*(\eta)\rangle$, and the variance is equal to one, $R(0) = 1$. Noting that the first integral in Eq. (16) yields the fiber length, $z$, and that the autocorrelation function contributes only over the order of the correlation length, Eq. (16) is rewritten as

$$P_m(z) = zP_n(0)\frac{K_{mn}^2}{2} \int_{-\infty}^{\infty} \exp(j\Delta\beta'_{mn}\zeta)R(\zeta)d\zeta \tag{17}$$

Finally, we obtain the following longitudinally varying, local PCC with the power spectral density, $S(\Delta\beta'_{mn})$, which is the Fourier transform of the autocorrelation function:

$$h_{mn} = \frac{P_m(z)}{zP_n(0)} = \frac{K_{mn}^2}{2}S(\Delta\beta'_{mn}) \tag{18}$$

Here, we consider three types of autocorrelation functions, exponential autocorrelation function (EAF),

$$R(\zeta) = \exp\left(-\frac{|\zeta|}{d_c}\right) \tag{19}$$

Gaussian autocorrelation function (GAF),

$$R(\zeta) = \exp\left[-\left(\frac{\zeta}{d_c}\right)^2\right] \tag{20}$$

and triangular autocorrelation function (TAF)

$$R(\zeta) = \begin{cases} 1 - \dfrac{|\zeta|}{d_c}, & |\zeta| \le d_c \\ 0, & |\zeta| > d_c \end{cases} \tag{21}$$

where $d_c$ is the correlation length. The corresponding PCCs are, for EAF,

$$h_{mn}(z) = \frac{K_{mn}^2 d_c}{1 + \left[\Delta\beta'_{mn}(z)d_c\right]^2} \tag{22}$$

for GAF,

$$h_{mn}(z) = \frac{\sqrt{\pi}K_{mn}^2 d_c}{2}\exp\left\{-\left[\frac{\Delta\beta'_{mn}(z)d_c}{2}\right]^2\right\} \tag{23}$$

and for TAF,

$$h_{mn}(z) = \frac{K_{mn}^2 d_c \sin^2\left[\Delta\beta'_{mn}(z)d_c/2\right]}{2\left[\Delta\beta'_{mn}(z)d_c/2\right]^2} \tag{24}$$

where $\Delta\beta'_{mn}(z)$ is the local propagation-constant difference defined as Eq. (12). In the earlier CPT [3–5], the following local PCC was adopted:

$$h_{mn}(z) = \frac{4K_{mn}^2}{\pi\sqrt{4K_{mn}^2 + \left[\Delta\beta'_{mn}(z)\right]^2}} \tag{25}$$

which is defined as the ratio of maximum power-conversion efficiency to coupling length. EAF and GAF have been introduced to microbending-loss analysis [11,12].

*3.2 Simulation results*

Figure 5 shows the bending-diameter dependence of crosstalk in the quasi-homogeneous 7-core fiber (see Fig. 3) calculated by CPT with EAF. In this figure, the results of the earlier CPT based on Eq. (25) [4] are also plotted. In the phase-matching region, the crosstalk is independent of the correlation length. In the non-phase-matching region, on the other hand,

the crosstalk is strongly dependent on the correlation length. As in CMT with segment length of 0.05 m, the simulation results with correlation length of 0.05 m agree well with the measurement results [4] and therefore, the correlation length of this fiber is thought to be 5 cm or so.
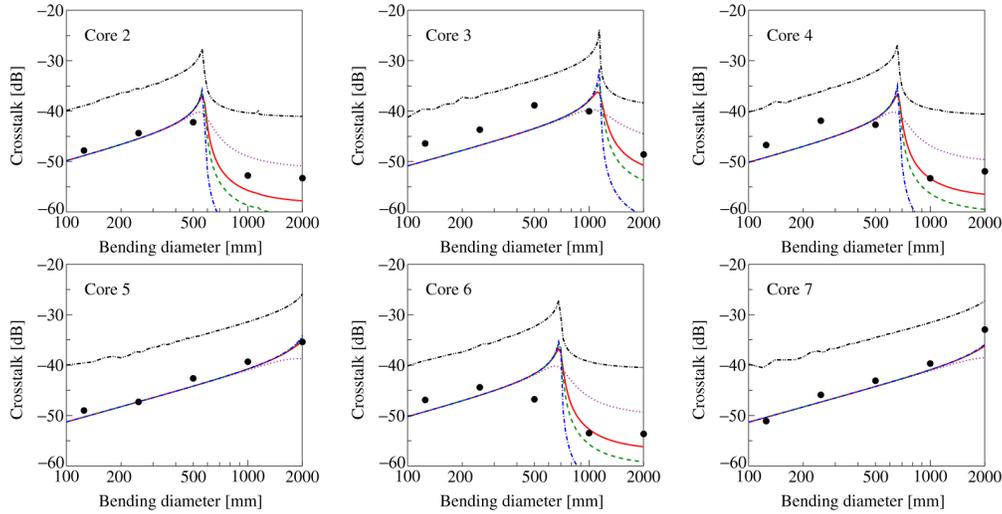


Fig. 5. Bending-diameter dependence of crosstalk calculated from coupled-power theory with exponential autocorrelation function. Dotted line: $d_c = 0.01$ m, solid line: $d_c = 0.05$ m, dashed line: $d_c = 0.1$ m, dashed and dotted line: $d_c = 0.5$ m, dashed and double-dotted line: Eq. (25) [4], closed circles: measured data [4].

Figure 6 shows the propagation-distance dependence of PCCs between center core and outer cores for the bending diameter of 250 mm. We can see that the phase-matching resonances do occur in all cores. The average values of PCCs over the twist pitch, in this case, 20 m, are almost the same for all the correlation lengths. This is the reason why in the phase-matching region, the crosstalk is independent of the correlation length.

In Fig. 7, the bending diameter is taken as 1,000 mm. The phase-matching resonances do not occur in cores 2, 4, and 6, and the average values of PCCs over the twist pitch are decreased with increasing correlation length, resulting in the correlation-length dependence of crosstalk in the non-phase-matching region.
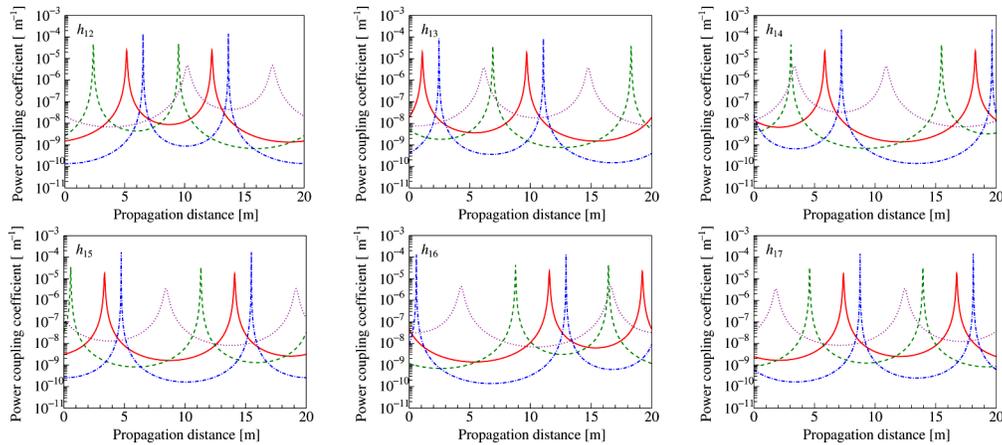


Fig. 6. Propagation-distance dependence of power-coupling coefficients for bending diameter of 250 mm. Dotted line: $d_c = 0.01$ m, solid line: $d_c = 0.05$ m, dashed line: $d_c = 0.1$ m, dashed and dotted line: $d_c = 0.5$ m.
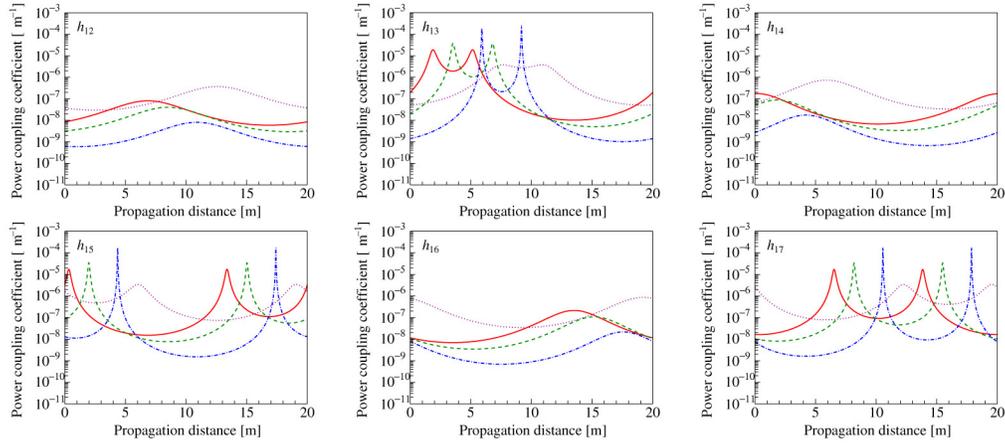
Fig. 7. Propagation-distance dependence of power-coupling coefficients for bending diameter of 1,000 mm. Dotted line: $d_c = 0.01$ m, solid line: $d_c = 0.05$ m, dashed line: $d_c = 0.1$ m, dashed and dotted line: $d_c = 0.5$ m.

Figure 8 shows the simulation results obtained by CPT with GAF. The crosstalk behaviors are well simulated in the phase-matching region because in this region, the crosstalk is independent of statistical properties. However, in the non-phase-matching region, the crosstalk behaviors are not well simulated.

The simulation results in Fig. 9 are obtained by CPT with TAF and surprisingly, are in excellent agreement with those of CMT (see Fig. 4). In CMT, in order to obtain sufficiently accurate average values of crosstalk, we should simulate a large number of samples, in this simulation, 100 samples. In CPT, on the other hand, the average crosstalk values can be obtained by only one simulation.
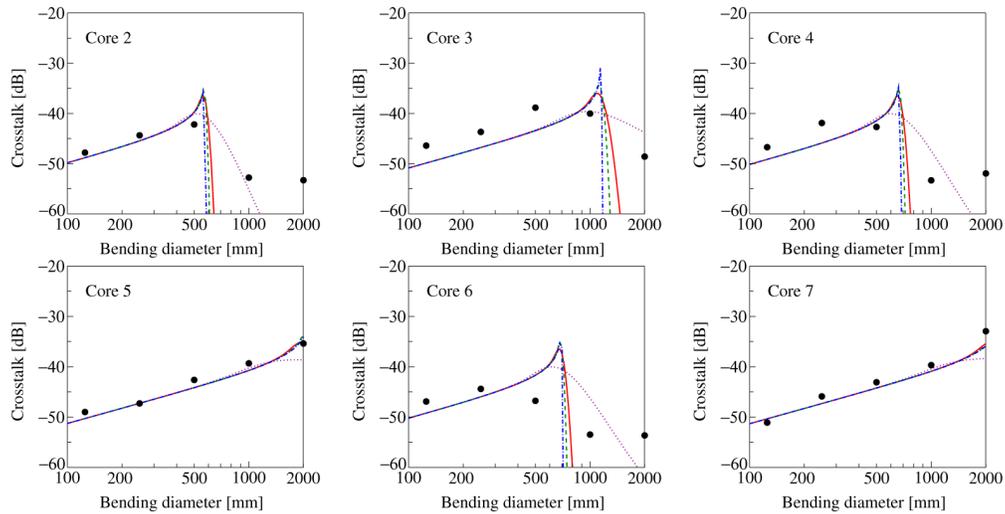


Fig. 8. Bending-diameter dependence of crosstalk calculated from coupled-power theory with Gaussian autocorrelation function. Dotted line: $d_c = 0.01$ m, solid line: $d_c = 0.05$ m, dashed line: $d_c = 0.1$ m, dashed and dotted line: $d_c = 0.5$ m, closed circles: measured data [4].
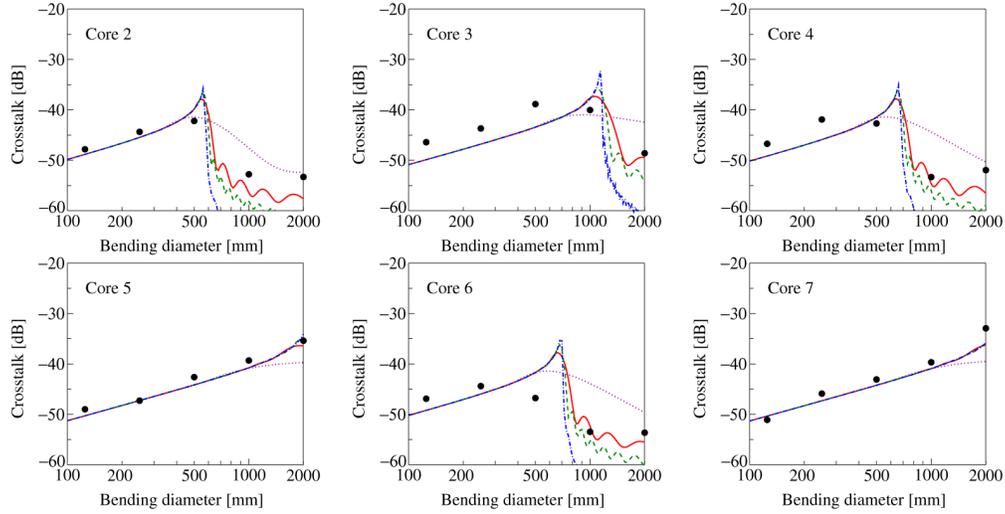
Fig. 9. Bending-diameter dependence of crosstalk calculated from coupled-power theory with triangular autocorrelation function. Dotted line: $d_c = 0.01$ m, solid line: $d_c = 0.05$ m, dashed line: $d_c = 0.1$ m, dashed and dotted line: $d_c = 0.5$ m, closed circles: measured data [4].

Finally, in order to check whether the reciprocity is satisfied in MCFs or not, the simulation results obtained by CMT and CPT with TAF are shown in Figs. 10 and 11, respectively. The left figures show the crosstalk between center core 1 and outer core 4, the middle figures show the crosstalk between center core 1 and outer core 5, and the right figures show the crosstalk between outer cores 4 and 5. From these results, we can see that the reciprocity is satisfied.
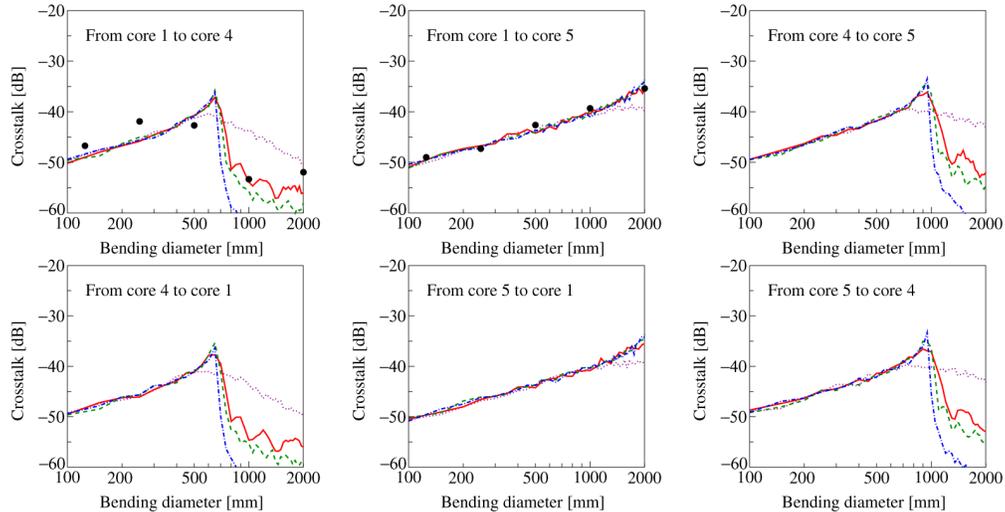


Fig. 10. Bending-diameter dependence of crosstalk calculated from coupled-mode theory. Left figures: from core 1 to core 4 (top) and from core 4 to core 1 (bottom), middle figures: from core 1 to core 5 (top) and from core 5 to core 1 (bottom), right figures: from core 4 to core 5 (top) and from core 5 to core 4 (bottom). Dotted line: $d_c = 0.01$ m, solid line: $d_c = 0.05$ m, dashed line: $d_c = 0.1$ m, dashed and dotted line: $d_c = 0.5$ m, closed circles: measured data [4].
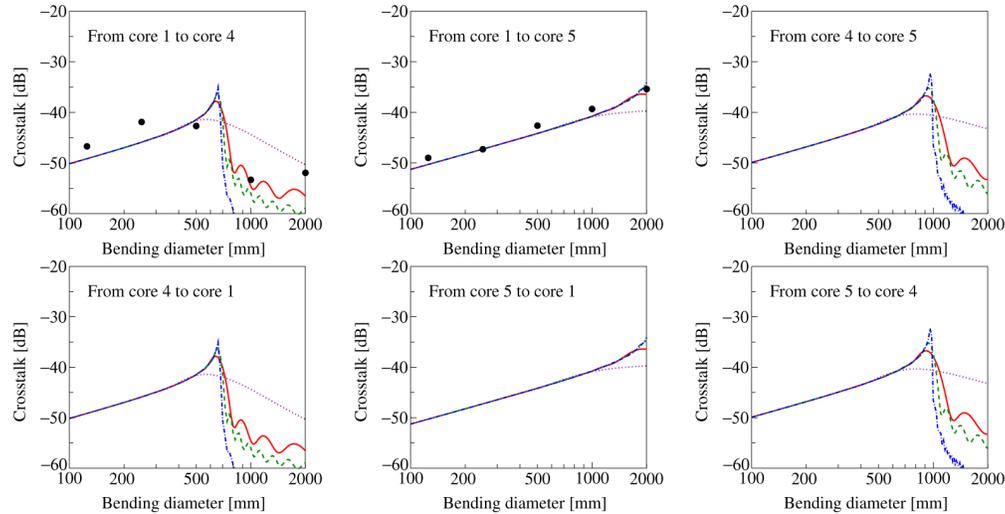
Fig. 11. Bending-diameter dependence of crosstalk calculated from coupled-power theory with triangular autocorrelation function. Left figures: from core 1 to core 4 (top) and from core 4 to core 1 (bottom), middle figures: from core 1 to core 5 (top) and from core 5 to core 1 (bottom), right figures: from core 4 to core 5 (top) and from core 5 to core 4 (bottom). Dotted line: $d_c = 0.01$ m, solid line: $d_c = 0.05$ m, dashed line: $d_c = 0.1$ m, dashed and dotted line: $d_c = 0.5$ m, closed circles: measured data [4].

## 4. Conclusion

Coupled-mode and coupled-power theories were revised for multi-core fiber design and analysis. First, to satisfy the law of power conservation, the mode-coupling coefficients were redefined. Then, the closed-form power-coupling coefficients were derived based on exponential, Gaussian, and triangular autocorrelation functions. The coupled-power theory is effective for investigating the crosstalk behaviors in multi-core fibers and especially, the triangular autocorrelation function works well. It was shown that the statistical properties of bent multi-core fibers are different between the phase-matching region and the non-phase-matching region. The correlation length for which we have no reliable information can be predicted by comparing the results of coupled-power theory with the measurement results. Furthermore, from the simulation results obtained by both theories, it was confirmed that the reciprocity is satisfied in multi-core fibers.